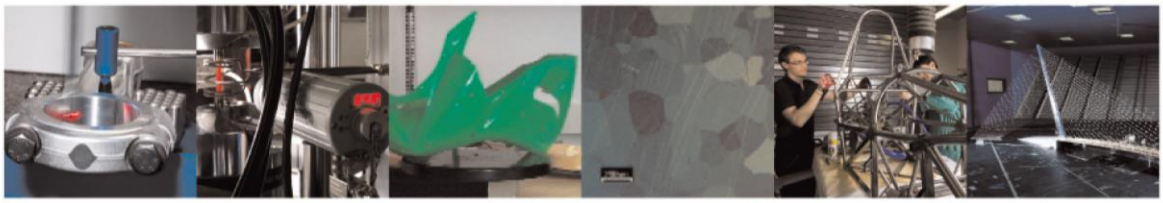

Control of an integrated lateral and roll suspension for a high-speed railway vehicle

Egidio Di Gialleonardo, Alan Facchinetti & Stefano Bruni

This is a post-peer-review, pre-copyedit version of an article published in Vehicle System Dynamics. The final authenticated version is available online at:
http://dx.doi.org/10.1080/00423114.2022.2049319

DIPARTIMENTO DI MECCANICA ■ POLITECNICO DI MILANO
via G. La Masa, 1 ■ 20156 Milano ■ EMAIL (PEC): pecmecc@cert.polimi.it
http://www.mecc.polimi.it
Rev. 0

Control of an integrated lateral and roll suspension for a high-speed railway vehicle

Egidio Di Gialleonardo, Alan Facchinetti, and Stefano Bruni

Abstract

This paper proposes the combined control of lateral and roll carbody motion to improve ride quality in a high-speed train during curve negotiation. The active suspension consists of an active anti-roll device based on hydraulic interconnected actuators and on a hydraulic active lateral suspension. Three control strategies are proposed and the parameters defining the control laws are defined using Genetic Algorithm optimisation, with ride quality estimation performed based on numerical simulation of the curving behaviour of the active vehicle. The performance of the vehicle in passive configuration and with the active suspension is also assessed using numerical simulation, showing that the use of combined lateral and roll control enables the vehicle to run at 340 km/h providing the same or even higher level of ride quality as the passive vehicle running at 300 km/h. Simulation results also provide an estimate of the mechanical power required to operate the active suspension and prove that the use of active control is neutral towards running safety.

1 Introduction

The introduction of active capabilities in the suspensions of railway vehicles is recognised as a means to improve their performances, in terms of stability, wear, reduced damage to the infrastructure and increased ride quality compared to a vehicle with passive suspensions. Hence, a number of papers and different surveys analysing the development and the implementation of active suspension systems in railway engineering can be found in the scientific literature [1–4].

Among others, tilting body systems were developed [5], aimed at increasing the vehicle speed through curves, taking advantage from the fact that the speed limit in curves is usually associated to passenger comfort rather than to running safety. In fact, the possibility of tilting the carbody inwards provides a reduction of the acceleration felt by the passengers, thus permitting to increase the speed.

Most existing tilting body systems for railway vehicles resort to rather bulky and heavy mechanical linkages to achieve large tilt angles [6], leading to increased vehicle weight and reduced available space, even though some attempts have been made to obtain reduced angles without modifying the classical architecture of the bogie, for example by means of controlling the airspring [7,8]. The latter systems are designed especially for high-speed vehicle applications, that are characterised by severe constraints in terms of axle loads and space available for passengers, usually non compatible with systems providing large tilting angles.

The main drawback of tilting body systems based on active airspring control lies in the heavy consumption of pressurised air which is required to operate this system, causing a poor energy efficiency of the active system and requiring the over-sizing of air compressors in the train set. Therefore, the authors of this paper proposed previously the adoption of an active anti-roll device based on hydraulic interconnected suspensions [9] which retains the advantages of tilt actuation based on active air springs whilst removing the drawbacks mentioned above. One advantage of the solution proposed in [9] is that the system can be designed to behave as a classical anti-roll bar when operated in passive mode.

Tilting systems are generally associated with an active lateral suspension in order to compensate for the larger lateral displacement of the carbody due to the increased speed and to avoid gauging issues. Additionally, the active lateral suspension may be used to prevent bumpstop contact at the secondary suspension level, thus improving ride comfort while negotiating a curve [10]. However, to the best of the authors' knowledge, there are only few examples of full integration of tilting devices and active lateral suspensions[11], even though the combination and integration of the two subsystems may lead to significant improvements in the performance of the active system because the structural coupling of carbody roll and lateral motion components can be accounted for. The target of the integrated system may be, for example, the improvement of ride comfort, especially related with the mitigation of motion sickness.

Aim of this work is the development and the numerical testing of a fully integrated active system composed by an active anti-roll device, based on hydraulic interconnected suspensions, coupled to a hydraulic active lateral suspension. The two subsystems are controlled simultaneously according to different control strategies. In particular, the effectiveness of classical PID schemes, also in association with a sky-hook contribution is investigated, and an optimal linear quadratic (LQ) regulator is considered as an alternative.

The optimisation of the PID regulator can be performed using typical tuning rules of control theory, like Ziegler-Nichols method or other approaches based on a popular set of metrics in process control applications [12,13] which have been also used in the framework of active suspension systems [14] and active tilting trains [15,16]. However, due to the nonlinear nature of the system and to the presence of multiple conflicting objectives, a multi-objective genetic algorithm is employed here, considering performance indicators related to both reference tracking and ride comfort. The same approach is adopted for the tuning of the LQ regulator.

The main contribution of this paper is a comprehensive assessment of the benefits provided by the integration of tilt and lateral suspension control in regard to passenger comfort and to motion sickness reduction. This is obtained using a fully non-linear vehicle model which accounts for the non-linear effects in wheel/rail contact, the dynamics of the actuation system, the estimation process for the quantities required by the control system and the possible uncertainties associated with the positioning system.

The paper is organised as follows. The concept of the active system and the modelling and dimensioning of the actuation system are presented in section 2. Section 3 is devoted to the description of the controllers in terms of definition of the control strategies, of the references and of the measurements needed for control loop closure. As already mentioned, the selection of the controller gains is performed using an optimisation procedure based on multi-objective genetic algorithm. The assessment of the objective functions is performed using a non-linear multi-body model of the vehicle which also accounts for the dynamics of the actuation system, The complete model of the active vehicle and the optimisation tool are briefly described in section 4. Section 5 compares the results of the different strategies in terms of their performances, running safety of the vehicle and power consumption in the actuation system. The robustness with respect to positioning errors is also investigated. Some concluding remarks are finally given in section 6.

2 Concept and dimensioning of the active system

The active system considered in this study can be seen as composed by two parts that are integrated and controlled simultaneously:

- an active anti-roll device;
- an active lateral suspension.

The active system is designed with three main objectives:

- provide the same carbody-bogie roll and lateral stiffness as a conventional anti-roll device and lateral suspension, when the system is operated in passive mode;
- actuate the desired carbody tilt angle when the vehicle negotiates a curve;
- enhance vehicle performances compared to a vehicle equipped with passive suspensions, particularly in respect to passenger comfort, i.e. improve the ride quality for the same speed or maintain the ride quality level when the speed is increased.

The scheme of the anti-roll device is based on hydraulically interconnected double-action cylinders. The system was developed mainly for automotive applications [17] and was described in more details in [9].The concept is modified, with respect to the passive system, introducing a servo-valve and a pump into the circuit, that are used for controlling the fluid flow to the reservoirs of the two actuators (Figure 1 (a)). The red colour is adopted for representing the high-pressure line of the hydraulic circuit, whereas the blue colour for the low-pressure line.

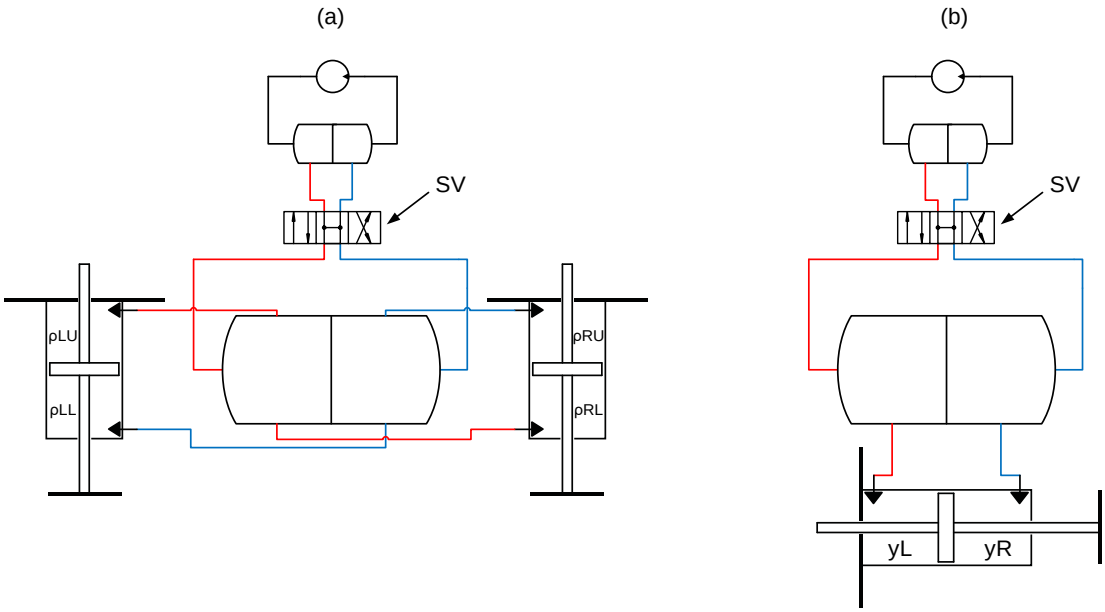

Figure 1. Layout of the hydraulic anti-roll device (a) and of the hydraulic active lateral suspension (b).

The active lateral suspension is also realised by a hydraulic circuit where a hydraulic actuator is controlled using an additional servo-valve (Figure 1 (b)).
The active function is activated when the vehicle negotiates a curve, imposing a specified tilt angle to the carbdoy and keeping the lateral position centred with respect to the bumpstops. The speed and position of the vehicle as well as the parameters of the curve being negotiated are assumed to be known to the control system from a reference

generation unit based on geo-localisation of the train in combination with a line database providing information on track curvature and cant as function of the position.

2.1 Model of hydraulic actuators

The actuator models are based on fluid dynamic equations using the following assumptions:

- the flow is laminar and mono-dimensional;
- losses due to fluid viscosity are neglected;
- the fluid is in isothermal conditions;
- the fluid is partially compressible in the actuator chambers and related additional reservoirs, whereas it is incompressible in the pipes;
- the pressure in the supply and return reservoirs are constant;
- the mass of the piston and of the piston rod are negligible;
- the servo-valves are assumed to behave as a first-order system.

The same modelling approach has been already used in [9] where the active anti-roll device hydraulic model was introduced. Applying the laws of conservation of mass and considering the mentioned hypotheses, it is possible to derive a non-linear model of the generic actuator as:

$$\begin{cases} \left(\frac{V_0}{\beta} + \frac{A\,x}{\beta}\right)\dot{p}_1 + (c_i + c_e)p_1 - c_i p_2 = -A\dot{x} + Q_{s1} \\ \left(\frac{V_0}{\beta} - \frac{A\,x}{\beta}\right)\dot{p}_2 - c_i p_1 + (c_i + c_e)p_2 = +A\dot{x} + Q_{s2} \end{cases} \tag{1}$$

where p_1 and p_2 are the pressure inside the two sides of the considered hydraulic system (the two branches of circuit for the active anti roll device or the two chambers of the actuator for the active lateral suspension), x is the displacement of the piston relative to the cylinder, β is the bulk modulus, A is the area of the piston/s, c_i and c_e are the internal and external leakage coefficients [18], Q_{s1} and Q_{s2} are the flows from the servo-valve in the two branches of the hydraulic circuit (positive when incoming).
For each one of the three hydraulic actuators included in the active suspension (two for the tilt system and one for the lateral suspension) the displacement x of the piston relative to the cylinder can be expressed as a function of the vehicle's coordinates.
When considering the active lateral suspension, $x = x_y$ is the displacement of the corresponding hydraulic actuator and $V_0 = V_{y0}$ is the total fluid volume when the lateral suspension is in the reference position.
On the other hand, when considering the active anti-roll device, $x = 2\frac{b_\rho}{2}\Delta\rho$ is twice the displacement of the single hydraulic actuator, with $\Delta\rho$ the relative carbody-bogie roll, and $V_0 = 2V_{\rho 0}$ is the fluid volume in the main circuit (twice the volume of each branch), on account of the interconnection between the two branches (see Figure 1) [9]. In this case, the leakage coefficients are obtained considering the contributions of both actuators.
The actuators are interfaced to the servo-valves governing the flows Q_{s1} and Q_{s2} and to the vehicle. The servo-valves are modelled using non-linear equations, as the pressure jump across the valves depends on the state of the spool valve. The equation for the two sides of the hydraulic circuit is:

$$Q_{s1,2} = \begin{cases} C_s(x_s) d_s x_s \sqrt{\dfrac{2(p_S - p_{1,2})}{\rho_o}} & \text{for fluid supply} \\ -C_s(x_s) d_s x_s \sqrt{\dfrac{2(p_{1,2} - p_R)}{\rho_o}} & \text{for fluid return} \end{cases} \tag{2}$$

In (2) C_s is the efflux coefficient, which depends on the spool position x_s; d_s is the constant length parameter of the valve, p_S is the supply pressure and p_R is the return pressure in the feeding circuit (as mentioned above, these quantities are assumed to be constant during the simulation); ρ_o is the density of the oil. The spool position x_s is an additional state variable of the actuator and directly depends on the controller command u_s considering a finite response time according to the 1-st order model:

$$\dot{x}_s + \frac{1}{\tau_s} x_s = \frac{k_s}{\tau_s} u_s \tag{3}$$

where τ_s is the time constant of the servo-valve and k_s is a gain representing the steady-state position of the spool for unit command.
The actuators generate two equal and opposite moments and forces on the bogie and the carbody (Figure 2):

$$\begin{aligned} F_\rho &= A_\rho (p_{\rho 1} - p_{\rho 2}) \\ F_y &= A_y (p_{y1} - p_{y2}) \end{aligned} \tag{4}$$

2.2 Dimensioning of the actuation system

The first step in the definition of the active system is the dimensioning of the components, mainly the actuators, so that they meet the requirements of the active suspension in terms of forces to the vehicle and equivalent stiffness when the system is operated in passive mode. This is important in order to guarantee the correct rejection of disturbance arising from lateral and cross-alignment track irregularities.

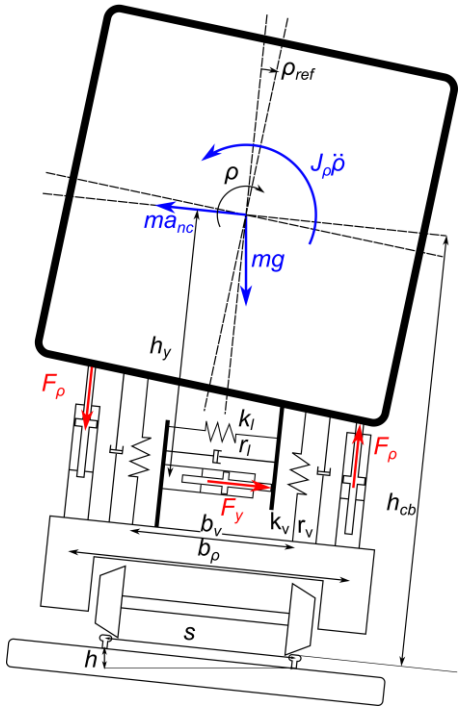

Figure 2. Forces on the carbody during curve negotiation.

Using simple equilibrium equations and neglecting the deformations of the primary suspension, it is possible to evaluate the steady forces $F_{\rho 0}$ and F_{y0} to be generated respectively by roll actuators and by the lateral actuator to correctly perform the tilting manoeuvre (see Figure 2):

$$F_{\rho 0} = \frac{J_\rho \ddot{\rho}_{ref} + m a_{nc} h_y + k_v \frac{b_v^2}{2} \rho_{ref} - mg \rho_{ref} h_{cb}}{b_\rho} \qquad (5)$$

$$F_{y0} = m a_{nc}$$

where m and J_ρ are respectively the mass and the roll moment of inertia of the half-carbody, k_v is the vertical stiffness of the secondary suspensions and b_v is their lateral distance, b_ρ is the distance between the actuators of the anti-roll device, h_{cb} is the height of the centre of mass of the carbody with respect to the top of the rail and h_y is the distance between the same point and the active lateral suspension. Finally, $\ddot{\rho}_{ref}$ is the reference angular acceleration in roll prescribed for the carbody, which is non-zero along the curve transitions (see section 3.1) and a_{nc} is the non-compensated lateral acceleration, i.e. the difference between the centripetal acceleration and the compensation provided by track cant $a_{nc} = \frac{V^2}{R} - g\frac{h}{s}$, with V the vehicle forward speed, R the curve radius, h the track cant, s the lateral distance between the rails and g the gravity acceleration.

The supply and return pressures of the hydraulic circuit are set to 198 bar and 2 bar respectively, corresponding to a maximum available pressure drop of 196 bar. Assuming a maximum force of 40 kN for roll actuators and of 50 kN for the lateral actuator, the area of the pistons are obtained, as reported in Table 1.
The equivalent stiffness in roll and in lateral direction, k_ρ and k_y respectively, are obtained assuming the servo-valve to be set to the fully open position and neglecting oil leakage from one chamber to the other. The following expressions are found, see Appendix 1 for the derivation of these expressions:

$$k_\rho = \frac{A_\rho^2 b_\rho}{V_{\rho 0}} \beta$$
$$k_y = 2\frac{A_y^2}{V_{y0}} \beta \tag{6}$$

In order to tune the equivalent stiffness of the active system to the same value as the passive vehicle, additional reservoirs should be added to the hydraulic circuit so to increase the volume of the chambers.
Table 1 reports the geometrical data for the actuators chosen together with the value of the equivalent stiffness.

	Anti-roll device	Lateral suspensions
Stroke [mm]	240	200
Piston Area A [mm^2]	1964	2502
Volume V_0 [dm^3]	7.97	15.3
Equivalent stiffness	1367.5 Nm/mrad	902.7 N/mm

Table 1. Main characteristics of the actuators and of the hydraulic circuits for the active anti-roll device and lateral suspension.

3 Design of controllers

As already mentioned, the mechatronic system developed in this work is made up of two parts, the active anti-roll device and the active lateral suspension, that are controlled simultaneously.
However, the objectives of the two subsystems are slightly different:

- as far as the roll motion of the carbody is concerned, the active system should accomplish the tracking of a reference tilt angle, which is supposed to be known as a function of speed and of the curve being negotiated;
- considering the relative lateral motion between the carbody and the bogie, the controller is asked to perform a vibration control, keeping the carbody centred with respect to the bogie at the actuator level. In this case, the main goal is not tracking a desired trajectory for the carbody, but rather prevent the carbody from getting in contact with the bumpstop, thus improving the vibrational behaviour and, therefore, the perceived comfort.

To perform the above-stated tasks, three alternative control strategies are considered:

- feed-forward + PID feed-back (PID);
- feed-forward + PID feed-back + Sky-Hook damping (PIDSH);
- Linear Quadratic controller with the addition of an integral feedback action to track the tilt and lateral displacement references (LQ).

It is worth noting that the first two control strategies envisage a feed-forward contribution to guarantee a fast response of the active system and a feed-back contribution in order to compensate for un-modelled effects and uncertainty of the parameters. The LQ controller instead applies a classic state feedback strategy and does not resort to a feed-forward contribution.
In the following, the definition of the control strategies are described in detail, together with the definition of the references and of the measurements and estimations needed for feedback purposes.

3.1 Definition of the references

The references to be fed into the control system are defined under the assumption that the vehicle is equipped with a geolocalisation system [19,20], so that the controller has exact knowledge of the actual position of the vehicle along the track.
The tilt angle to be imposed to the vehicle in full curve is computed based on the maximum desired non-compensated lateral acceleration, which in turn depends on the curve geometry and on the vehicle speed. Assuming that both track curvature and cant vary linearly in curve transitions, the desired tilt angle results in a trapezoidal profile as a function of the position along the curve (Figure 3 (a)).
In lateral direction the controller should perform a vibration control and the reference value of the relative displacement between the carbody and the bogie at the bumpstop level is therefore null (Figure 3 (b)). In Figure 3 s_{ini1}, s_{out1}, s_{ini2}, s_{out2} are the start/end positions of the entry/exit transitions in the curve.

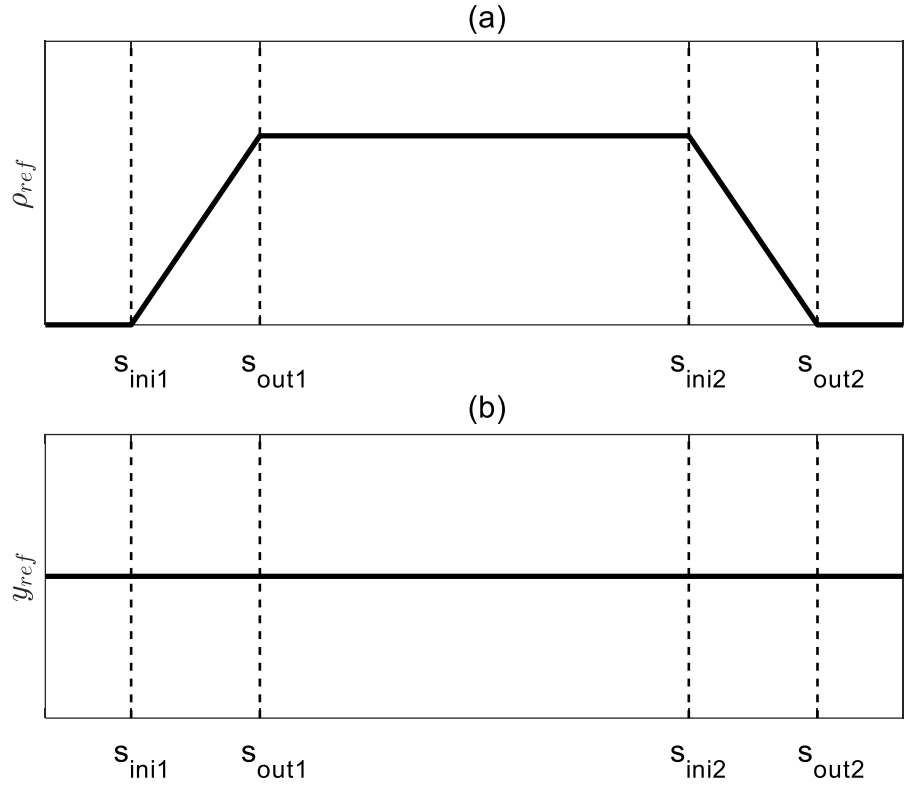

Figure 3. References for the tilt angle (a) and the lateral relative displacement between the carbody and the bogie at the bumpstop level (b) along a curve.

3.2 Feed-forward contribution for the PID and PIDSH controllers

All the considered controllers, with the exception of the LQ one, present a feed-forward contribution. In fact, assuming that the position and speed of the vehicle are known from a geo-localisation system and that track geometry is available from a data-base, it is possible to implement such contribution in order to increase the speed of actuation of the active suspension. On the other hand, the feedback contribution is still needed to compensate the effect of disturbances, besides the errors in the definition of the feed forward term related to parameter uncertainty, positioning errors, etc.

The feed-forward action for tilt is defined based on equations (1) to (4), neglecting in Eq. (1) the terms related to fluid compressibility and leaving to the feedback contribution the task of compensating these effects. In this way, the feedforward action $u_{FF\rho}$ is defined as proportional to the time derivative of the reference tilt through coefficient $k_{FF\rho}$:

$$\begin{aligned} u_{FF\rho} &= k_{FF\rho}\dot{\rho}_{ref} \\ k_{FF\rho} &= \frac{A_\rho b_\rho}{K_{q\rho}} \\ K_{q\rho} &= \left(\frac{\partial Q(u_s, \Delta p)}{\partial u_s}\right)_0 \end{aligned} \tag{7}$$

with $K_{q\rho}$ a gain coefficient between the servo-valve command and the flow, obtained from the linearisation of equation (2) for a given pressure jump and neglecting the finite response time of the valve.
From the first line of Eq.7, it is noted that the feedforward action exists only during the negotiation of transition curves.
For the lateral direction, a different approach is adopted. In this case the feed forward action is intended to realise the quasi-static carbody centring. To this end the feed forward contribution is defined so to counterbalance the centrifugal force on the carbody due to curve negotiation.
Considering all the centrifugal force balanced by the lateral actuators, the necessary pressure difference Δp_y for each cylinder is:

$$\Delta p_y = \frac{m\, a_{nc}}{2A_y} \tag{8}$$

where m is the carbody mass and a_{nc} is the non-compensated lateral acceleration.
Considering actuator dynamics (see eq. (1) to eq. (4)), the feed forward contribution is made of two terms, proportional to the non-compensated lateral acceleration through coefficient k_{FFdy} and to its time derivative through coefficient k_{FFpy} respectively:

$$\begin{aligned} u_{FFy} &= k_{FFdy}\dot{a}_{nc} + k_{FFpy}a_{nc} \\ k_{FFdy} &= \frac{m\, V_{y0}}{4\beta\, K_{qy}\, A_y} \\ k_{FFpy} &= \frac{m\, c_{toty}}{2\, K_{qy}\, A_y} \end{aligned} \tag{9}$$

where c_{toty} is the overall leakage coefficient.

3.3 Feed-back contributions for the PID and PIDSH controllers

In the first control strategy two independent PID regulators are adopted, acting on the error between the reference tilt angle and the carbody-bogie relative roll and on the reference(null) and actual relative lateral displacement respectively:

$$\begin{aligned} u_{FB\rho} &= k_{P\rho}\left(\rho_{ref} - \Delta\rho\right) + k_{D\rho}\left(\dot{\rho}_{ref} - \Delta\dot{\rho}\right) + k_{I\rho}\int\left(\rho_{ref} - \Delta\rho\right)dt \\ u_{FBy} &= k_{Py}(-\Delta y) + k_{Dy}(-\Delta\dot{y}) + k_{Iy}\int(-\Delta y)\,dt \end{aligned} \tag{10}$$

where $u_{FB\rho}$ and u_{FBy} are the feedback actions to the active antiroll devices and active lateral suspensions and $\Delta\rho$ and Δy are the carbody-bogie relative roll and lateral displacement for each bogie.
The regulators' gains k_P, k_D and $k_I$are optimised by means of a Genetic Algorithm approach (section 4.2), based on multi-body system simulations.
The second strategy is characterised by two independent PID regulators, as the previous one, with the addition of Sky-Hook damping contributions aimed at reducing the level of carbody vibration due to curve negotiation and to track irregularity.

Considering that the hydraulic actuation system introduces an integrator in the transfer function from the controller command to the tilt angle of the carbody, the sky-hook damping contributions can be defined as proportional to the carbody roll and lateral accelerations, $\ddot{\rho}$ and $\ddot{y}$ respectively:

$$u_{FB\rho} = k_{P\rho}(\rho_{ref} - \Delta\rho) + k_{D\rho}(\dot{\rho}_{ref} - \Delta\dot{\rho}) + k_{I\rho}\int(\rho_{ref} - \Delta\rho)\,dt - k_{SH\rho}\ddot{\rho}$$
$$u_{FBy} = k_{Py}(-\Delta y) + k_{Dy}(-\Delta\dot{y}) + k_{Iy}\int(-\Delta y)\,dt - k_{SHy}\ddot{y} \quad (11)$$

Also in this case the control gains, including the ones associated to sky-hook damping contributions $k_{SH\rho}$ and k_{SHy}, are defined by means of GA optimisation (section 4.3).
Figure 4 shows the block diagram of the control strategy with feed-forward contributions, independent PID regulators and Sky-Hook damping. The first strategy, i.e. without Sky-Hook damping, can be obtained by simply setting to zero gains $k_{SH\rho}$ and k_{SHy}.

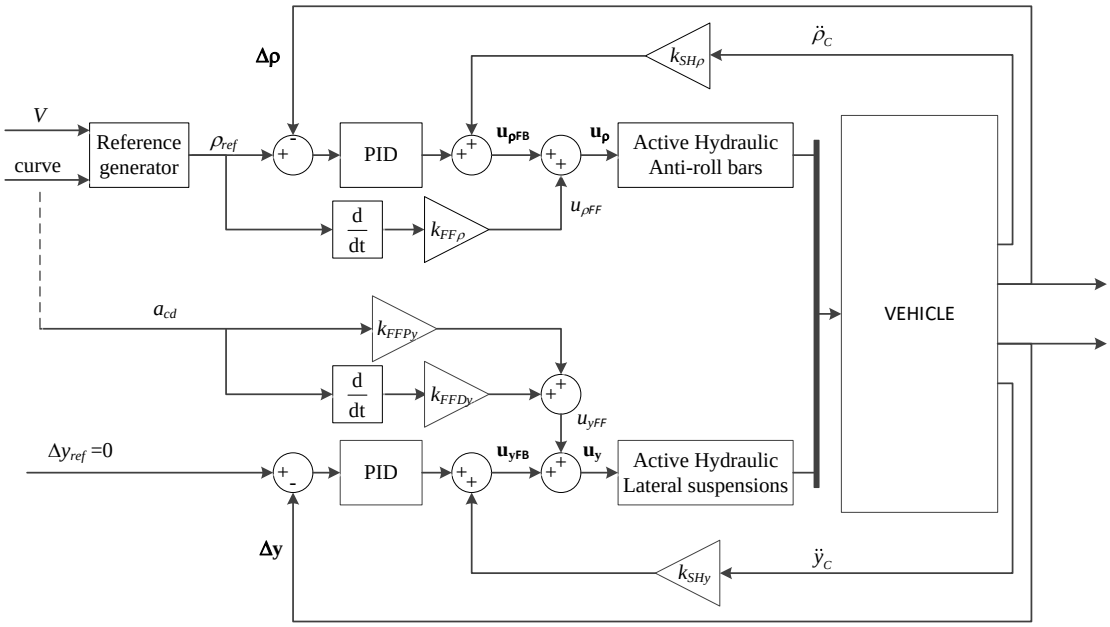

Figure 4. Block diagram of the feed-forward + PID feed-back regulator with Sky-Hook damping.

3.4 LQ controller

The last considered control strategy consists of a Linear Quadratic regulator, with the addition of integral feed-back actions to track the reference tilt and null carbody-bogie lateral displacement. The control scheme is reported in Figure 5.
The LQ regulator is defined using a simplified sectional model of the vehicle, see figure 2. This model considers the lateral and roll motion of the carbody and includes a simplified linearised representation of the dynamics of the hydraulic actuation system, whereas the dynamics of the bogie is neglected. The equations of the simplified model are presented in Appendix 2 The state-feedback gain matrix **K** and the integral gains collected in the diagonal matrix $\mathbf{K_I}$ are computed considering the infinite horizon LQ problem of minimising the cost function $\tilde{J}$:

$$\tilde{J} = \frac{1}{2}\int_0^{\infty} (\tilde{\mathbf{z}}^{\mathrm{T}}\,\mathbf{Q}\,\tilde{\mathbf{z}} + \mathbf{u}^{\mathrm{T}}\,\mathbf{R}\,\mathbf{u})dt \tag{12}$$

where $\mathbf{u}$ is the vector of control actions and $\tilde{\mathbf{z}} = [\mathbf{x} \quad \mathbf{x_I}]^{\mathrm{T}}$ is the augmented state vector consisting of union of the state vector $\mathbf{x}$ describing the dynamics of the simplified model shown in Figure 2 and of vector $\mathbf{x_I}$ defining the integrals of the tracking errors for the roll and lateral motion of the carbody:

$$\mathbf{x_I} = \int [(\rho_{\mathrm{ref}} - \Delta\rho) \quad (-\Delta y)]^{\mathrm{T}}\, dt \tag{13}$$

In this case, the GA optimisation is performed for the weight matrices $\mathbf{Q}$ and $\mathbf{R}$, which are assumed to be diagonal matrices.

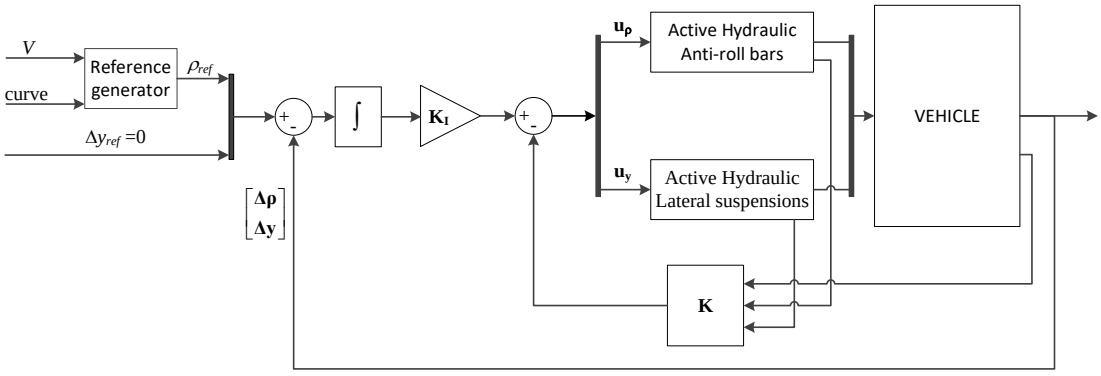

Figure 5. Block diagram of the Linear Quadratic regulator with integral actions.

3.5 Measurements and estimations for control feedback

The feed-back controllers require the availability of various measurements or estimations.

With reference to Figure 6, the carbody-bogie relative roll and lateral displacement required for the feedback of the PID controllers are evaluated from the measured displacements $x_{\rho 1}$ and $x_{\rho 2}$ of the hydraulic actuators in the active anti roll device and from the displacement x_y of the active lateral suspension:

$$\begin{cases} \Delta\rho = \dfrac{x_{\rho 1} - x_{\rho 2}}{b_\rho} \\ \Delta y = x_y + h_{yb}\Delta\rho \end{cases} \tag{14}$$

where h_{yb} is the vertical distance between the active lateral suspension and the lateral bumpstops.

The accelerations required for the evaluation of the Sky-Hook damping contributions are derived from the measurements a_{y1} and a_{y2} of carbody acceleration at two different heights, see Figure 6:

$$\begin{cases} \ddot{\rho} = \dfrac{a_{y2} - a_{y1}}{h_a} \\ \ddot{y} = a_{y1} + \ddot{\rho}\, h_{a1G} \end{cases} \tag{15}$$

being h_a the vertical distance between the two accelerometers and h_{a1G} the vertical distance between accelerometer 1 and the carbody centre of mass.

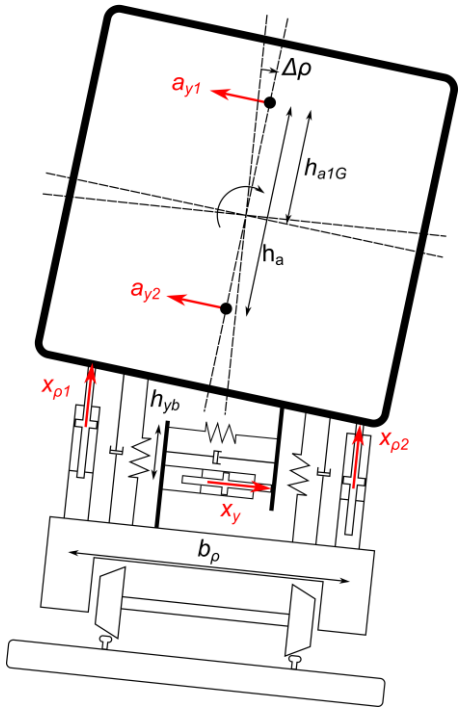

Figure 6. Position of displacement and acceleration sensors.

Velocity estimation is perfomed according to, the "Two-Channel Approach" proposed in [21]. Each velocity component of interest v^* is estimated as a weighted sum of the corresponding acceleration and displacement components, a and x respectively:

$$v^* = v_1^* + v_2^*$$

$$v_1^* = \frac{s^2}{s^2 + (\alpha_1 + \alpha_2)s + \alpha_1\alpha_2} a \qquad (16)$$

$$v_2^* = \frac{(\alpha_1 + \alpha_2)s^2 + \alpha_1\alpha_2 s}{s^2 + (\alpha_1 + \alpha)s + \alpha_1\alpha_2} x$$

where α_1 and α_2 are parameters of the method determining the frequency weightings as specified below.

For frequencies lower $\frac{\alpha_1}{2\pi}$ the velocity estimation is based almost exclusively on the measured displacement, while for frequencies higher than $\frac{\alpha_2}{2\pi}$ it is the measured acceleration that mostly contributes to the velocity estimation. In the frequency range from $\frac{\alpha_1}{2\pi}$ to $\frac{\alpha_2}{2\pi}$ the two measurements have approximately the same weight in affecting the estimation. In the considered application the transition was chosen to occur between

1 and 3 Hz, i.e. between the natural frequencies mainly related to carbody motion and those mainly related to bogie motion, resulting in $\alpha_1 = 2\pi \frac{\text{rad}}{\text{s}}$ and $\alpha_2 = 2\pi 3 \frac{\text{rad}}{\text{s}}$.

4 Dynamical models and optimization of the controllers

In this work, the choice of the values for the controller gains is not performed using classical approaches in control theory but is rather based on a multi-objective optimization accounting for conflicting objectives addressing at the same time tracking performances, ride quality and control effort. Among the available approaches for finding a solution of the problem, a multi-objective genetic algorithm (MOGA) is adopted.
To asses the performance of a given set of controller gains, the MOGA uses a non-linear multi-body systems (MBS) model of the vehicle with active suspension, in which the three control strategies described in Section 3 are implemented. This section presents the MBS model (sub-section 4.1) and illustrates the MOGA used for the optimisation of controller gains (sub-section 4.2).

4.1 Multi-body model of the railway vehicle

The complete model of the active vehicle used for the simulations can be divided into two parts: the multi-body model of the vehicle and the model of the active system comprising the actuators' model and the control system.
The complete railway vehicle model is defined using an in-house software that can be found in the literature under the name of ADTreS [22]. It is a simulation software for train-track interaction developed by the railway research group established at the Department of Mechanical Engineering of Politecnico di Milano and already employed to investigate many phenomena regarding train-track interaction. The software allows a rigid body schematisation of the carbody and the bogies, while as far as the wheelsets are concerned, a modal approach including the effect of flexibility can be used. For the sake of this work, being the objective of the analysis limited to low-frequency dynamics, a rigid body schematisation of the wheelsets is adopted.
The bodies are connected to each other by means of primary and secondary suspensions which are characterized by a set of linear and/or non-linear elements.
In total, the model comprises 35 degrees of freedom, five for each rigid body: vertical and lateral displacements, and three rotations (yaw, roll and pitch) are allowed. The forward motion is constrained to happen at constant speed V along the track.
Each independent coordinate of the vehicle is defined relative to a specific reference frame travelling at constant speed along track centreline. Three reference frames are used for the standard (one carbody - two bogies – four wheelsets) vehicle, one is relative to the carbody, and the other ones to the bogie assemblies.
Assuming that the bodies undergo small displacements relative to the moving reference, the kinematic relationships can be linearized; thus, the equations of motion can be written as:

$$\begin{aligned} \mathbf{M}_v \ddot{\mathbf{z}}_v + \mathbf{C}_v \dot{\mathbf{z}}_v + \mathbf{K}_v \mathbf{z}_v = \\ = \mathbf{F}_i(V,t) + \mathbf{F}_{nl}(\mathbf{z}_v, \dot{\mathbf{z}}_v) + \mathbf{F}_c(\mathbf{z}_v, \dot{\mathbf{z}}_v, V, t) \\ + \mathbf{F}_{act}(\mathbf{z}_v, \dot{\mathbf{z}}_v, \mathbf{z}_{act}, \dot{\mathbf{z}}_{act}, \mathbf{u}) \end{aligned} \tag{17}$$

where the vector $\mathbf{z}_v$ contains the independent coordinates of the system, $\mathbf{M}_v$, $\mathbf{C}_v$ and $\mathbf{K}_v$ are the vehicle's mass, damping and stiffness matrices. $\mathbf{F}_i$ is the vector of inertial forces due to the non-inertial motion of the moving references, $\mathbf{F}_{nl}$ consists of forces due to non-linear elements in the suspensions and $\mathbf{F}_c$ are the forces that the vehicle exchange with the track. $\mathbf{F}_{act}$ are the Lagrangian components of the forces generated by the actuators, i.e. the active anti-roll device and the active lateral suspension (as shown in subsection 2.1), which depend on the vehicle states, on the actuator states $\mathbf{z}_{act}$ and the controller outputs $\mathbf{u}$.
Wheel-rail contact forces are computed using a non-linear, multi-Hertzian contact model [23], considering the effect of track irregularities. These are generated from a random realisation of low-level irregularity ERRI spectra [24]. Given the frequency range considered in the model (5-10 Hz), track flexibility effects are neglected, as they have negligible effect in a frequency range up to 20 Hz [25] which is the focus of this work.
The complete set of equations is obtained by adding to eq. (17) the equations describing the hydraulic actuators' dynamics (subsection 2.1) and those relevant to the considered control strategy (section 3)

4.2 Optimisation tool

The three controllers mentioned in Sect. 3 have various parameters that need to be fine-tuned in order to guarantee optimised system-level performances. On the other hand, several reasons advise against using traditional optimisation strategies:

- the non-linear nature of the vehicle model;
- the presence of multiple, conflicting objectives;
- the large number of parameters to be optimized at the same time;
- the possible presence of local optima.

A multi-objective genetic algorithm (MOGA) was therefore chosen, as it is capable of coping with the four critical features mentioned above. This decision is also supported by previous literature in the field of control systems [26] and active suspensions [27–30]. Among the great variety of MOGAs, the NSGA-II [31] stands out as one of the first and most widely used, thanks to its ability to efficiently select the most promising solutions.
The objectives of the simulation can be clustered into three groups. The controller shall guarantee satisfactory ride quality for passengers, but, at the same time, the car body shall follow a trajectory compatible with the vehicle's dynamics and the power required to operate the actuators shall be sufficiently small to enable using a compact and energy efficient actuation system. For these reasons, the genetic algorithm aims to minimize the following six objective functions:

1. the P_{CT} index [32], as a measure of the potential discomfort suffered by passengers in curve transitions. This value represents the percentage of passengers that may feel discomfort and its value should be below 5%, to ensure satisfactory ride quality;
2. the rms value of the lateral acceleration $rms(\ddot{y})$, as a measure of the vibrational comfort of the passengers;

3. the maximum absolute error in trajectory tracking over the roll motion $max(\varepsilon_R)$, in order to evaluate the quality of the controlled anti-roll device per se;
4. the maximum absolute error in trajectory tracking over the lateral displacement $max(\varepsilon_L)$, in order to evaluate the quality of the lateral suspension per se;
5. the rms value of the anti-roll device control command $rms(x_{dR})$, as an indicator of the energy consumption of the roll actuator; this quantity is given in percentage terms with respect to the maximum command to the servo-valve (100% means a full-opening command);
6. the rms value of the lateral suspension control command $rms(x_{dL})$, as an indicator of the energy consumption of the lateral actuator; analogously to the anti-roll device command this quantity is provided in percentage terms with respect to the maximum command that can be fed to the servo-valve.

These six objectives are partially or completely in contrast one to the other; therefore, a compromise shall be sought inside the Pareto frontier produced by the MOGA.
In order to find the Pareto-optimal solutions, the MOGA works out a tuning of the controllers' parameters. These are of two kinds: as far as the PID and the PIDSH controllers are concerned, the algorithm changes directly the controller gains, see Eq. 10 and Eq. 11; in the case of the LQ controller, the optimizer modifies the elements of the state and control weighting matrices, see Eq. 12, which is then used for defining the gain matrix. This difference is one of the reasons for the less satisfactory results which are anticipated for the LQ controller, see Section 5.
The algorithm's parameters (Table 2) were fine-tuned manually thanks to an initial sensitivity analysis supported by the literature on the topic [33,34]. Particular care was devoted to the choice of the population size and the number of generations to be considered, in order to limit the resources required for the computation.

	PID	**PIDSH**	**LQ**
Variables to be optimized	6	8	14
Population	500	500	500
Generations	121	161	201
Selection type	Tournament without replacement (2 individuals)		
Crossover type	One point		
Crossover probability	0.8		
Mutation type	Polynomial (order 20)		
Mutation probability	0.1		

Table 2. list of NSGA-II parameters

5 Simulation results

The optimisation of controllers and the assessment of performances of the active suspensions was carried out considering a fictitious but realistic high-speed vehicle

running on a specified track section characterised by a curve with 5500 m radius and 105 mm cant that is typical of the Italian high-speed network. The length of the transition curves is 330 m.

5.1 Optimisation of the controllers

The output of the optimisation performed using the procedure described in section 4.2 is an optimal population, i.e. a group of non-dominated individuals in the sense of Pareto. Once defined the Pareto frontier, it is possible to select among the non-dominated individuals the solutions which better meet imposed requirements. A series of selection criteria, described in Table 3, are defined in order to identify a sub-set of the non-dominated solutions satisfying criteria related to the performance of the system and to the magnitude of the control action. In this way the analysis of the non-dominated solutions is restricted to a limited number of individuals, all ensuring good ride quality performance and, at the same time, a reasonable intensity of the control forces, thereby facilitating the final choice of a "best" control configuration. Given the conflicting nature of the objectives of the controller, the final choice of the "best" controller shall be based inevitably on the designer's experience.

P_{CT}	$rms(\ddot{y})$	$rms(x_{dR})$	$max(\varepsilon_R)$	$rms(x_{dL})$	$max(\varepsilon_L)$
< 3.5%	-	< 100%	< 15 mrad	< 100%	< 30 mm

Table 3. Selection criteria for the optimal solutions.

In particular, it was chosen to impose limits permitting to select controllers with good tracking capabilities (defined by the maximum values of the tracking errors ε_R and ε_L) and good performances in terms of comfort in curve transitions (defined by the P_{CT} index). Additionally, it was decided to select only controllers generating rms values of the commands below 100% (with respect to the maximum command), as this is the limit condition to avoid reaching the maximum opening of the servo-valves, which would result in unwanted saturation of the control force.
The final selection of the optimal controllers was made choosing the non-dominated individuals that provide the best performance in terms of P_{CT} and $rms(\ddot{y})$.
Figures 7-9 show some of the projections in 2-dimensions of the solutions found, for the PID, PIDSH and LQ controllers respectively. All the non-dominated individuals are reported (using grey dots), with the ones satisfying the selection criteria in Table 3 highlighted in black.
For each control strategy, the non-dominated individual selected as the best control configuration is shown using a blue diamond.
As far as the PID controller is concerned (Figure 7), it is possible to observe that the solutions minimising the roll tracking error also provide a low (close to minimum) value of lateral acceleration (see Figure 7a). On the other hand, Figure 7b shows that the PCT index is generally small for all the individuals (always smaller than 4.5 %) so the choice of the preferred solution can be directed mainly to reduce the roll tracking error and, as a consequence, the lateral acceleration.

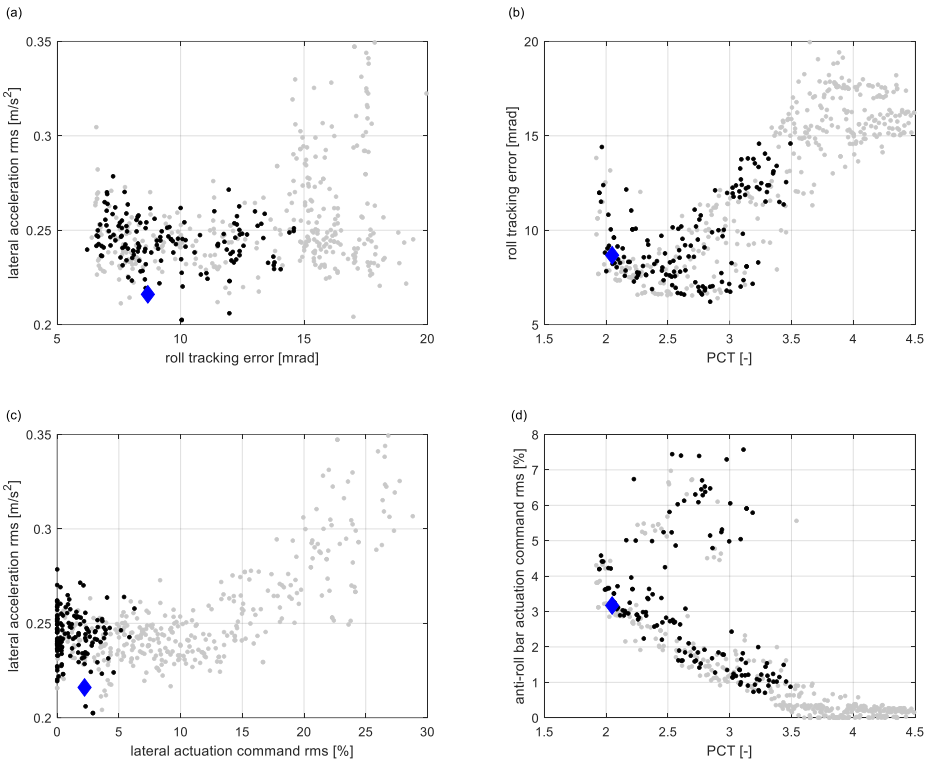

Figure 7. Projections in 2-dimension of the optimal solutions for the PID configuration. Grey dots: non-dominated individuals; black dots: non-dominated individuals satisfying the selection criteria; blue diamond: non-dominated individual selected as the best control configuration.

The addition of a sky-hook contribution increases the size of the problem, being the number of gains equal to 8, hence, as shown in Table 2, a larger number of generations are needed in order to define the Pareto frontier, whose projections in 2 dimensions are shown in Figure 8. Compared to the PID controller, PIDSH provides a large improvement in terms of attenuation of the lateral vibrations, reducing the rms of the lateral acceleration (Figure 8c). However, this improvement is traded for larger actuator commands, as can be observed comparing the Figure 8c and 8d with Figure 7c and 7d. As already shown for the simple PID controller, low levels of the PCT index can be easily achieved (Figure 8b and 8d) and, therefore, the selection of the optimal controller was driven by the performances in terms of lateral acceleration tracking.

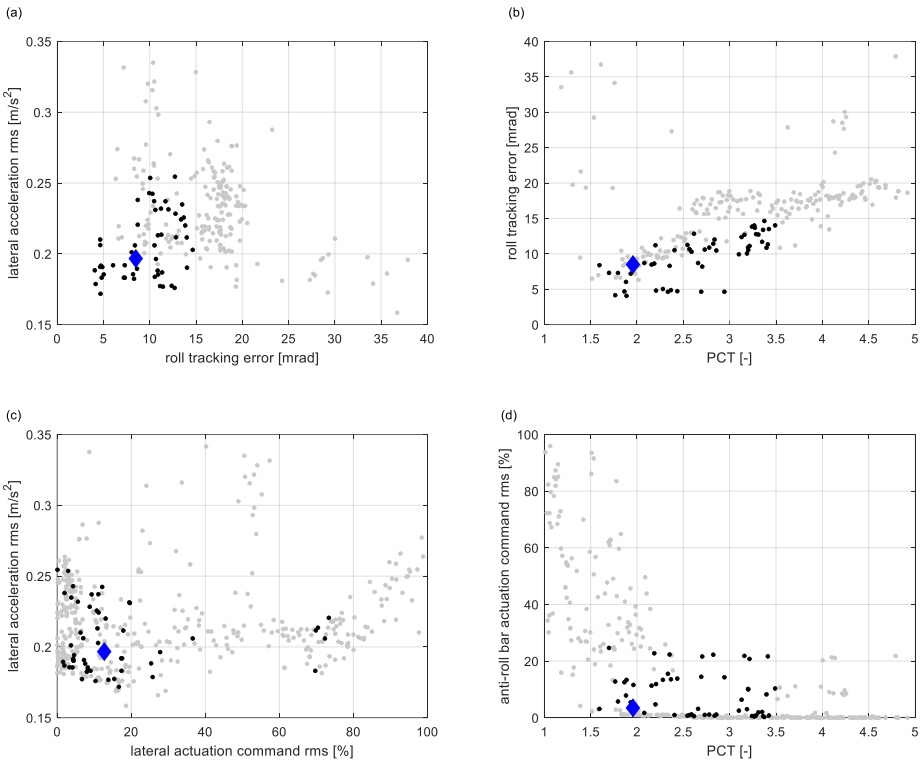

Figure 8. Projections in 2-dimension of the optimal solutions for the PIDSH configuration. Grey dots: non-dominated individuals; black dots: non-dominated individuals satisfying the selection criteria; blue diamond: non-dominated individual selected as the best control configuration.

The LQ controller is the most difficult to be optimised for two reasons: first, the size of the problem is further increased with respect to PID controller, since 14 variables are involved in the minimisation problem. Furthermore, the variables to be optimised are not directly the controller gains but the non-zero elements of the state and control weighting matrices in the algebraic Riccati equation. The results of the optimisation are shown in Figure 9.

In this case the solution was selected trying to minimise the levels of the actuators' commands, as it was noted that a further improvement of performance could be obtained only at the price of substantial increase of the control effort, as shown in Figure 9c and 9d.

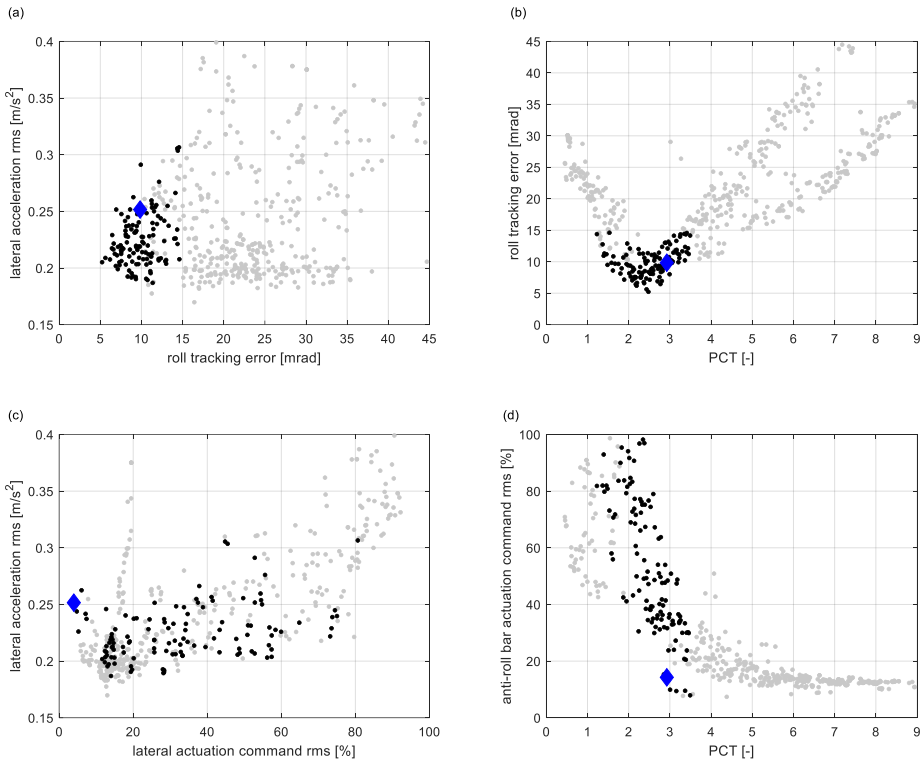

Figure 9. Projections in 2-dimension of the optimal solutions for the LQ configuration. Grey dots: non-dominated individuals; black dots: non-dominated individuals satisfying the selection criteria; blue diamond: non-dominated individual selected as the best control configuration.

5.2 Assessment of performance for the selected optimal controllers

As the final stage of the investigation, a performance assessment is carried out for the selected solutions of the multi-objective optimisation problem. Table 4 compares the values of the performance indexes for the selected optimal controllers. As a reference, the first two rows report the performance indexes of the vehicle in passive configuration negotiating the curve at 300 km/h (assumed service speed for the passive vehicle) and at 340 km/h (assumed increased speed made possible by the use of active suspensions). The increased speed value was chosen so to have the same quasi-static lateral acceleration perceived by the passengers for a vehicle running along a high-speed curve with a 2 deg. tilt angle and in a non-tilting vehicle running along the same curve at 300 km/h. This is considered a realistic speed increase for the high-speed application addressed here.

To provide a fair performance comparison for the active and passive vehicles, also the passive vehicle is considered equipped with an active lateral suspension (now in use on some HS trains). For this active suspension, a PI feedback controller is introduced, with gains tuned using the same strategy adopted for the integrated lateral+roll controller.

In order to assess the effectiveness of the integrated approach, Table 4 also reports the results obtained with the active roll suspension where the PID controller is optimised starting from the passive configuration, i.e. with the previously mentioned active lateral suspension, denoted as “PID (indip.)”. Thus, the PID (indip.) results are representative of a solution where both the lateral and roll suspension are active but tuned

independently. The reported results are different from those shown in [9] since in that case the whole active lateral suspension was represented as a simple first order system. It is worth noticing that this significant approximation is very favourable from the point of view of the resulting vehicle dynamics.
To avoid any confusion, the results referring to the active suspensions with integrated tuning are denoted with the addition of "(int.)"

Controller	P_{CT} **[%]**	$rms(\ddot{y})$ **[m/s^2]**	$rms(x_{dR})$ **[%]**	$max(\varepsilon_R)$ **[mrad]**	$rms(x_{dL})$ **[%]**	$max(\varepsilon_L)$ **[mm]**
Passive (V=300 km/h)	3.089	0.190	---	---	4.77-	18.8
Passive (V=340 km/h)	6.708	0.262	---	---	6.88	23.3
PID (indip.) (V=340 km/h)	2.220	0.217	5.76	8.9	3.93	21.0
PID (int.) (V=340 km/h)	2.049	0.216	5.50	8.7	2.99	24.5
PIDSH (int.) (V=340 km/h)	2.206	0.183	12.72	4.8	9.23	10.3
LQ (int.) (V=340 km/h)	2.926	0.252	13.54	9.8	3.42	20.9

Table 4. Performances of the optimised active system configurations.

The P_{CT} and $rms(\ddot{y})$ values obtained for the passive vehicle travelling at 340 km/h are considerably higher than the corresponding values obtained considering the vehicle running at 300 km/h and in particular the PCT value exceeds the maximum acceptable value of 5%. Therefore, it is concluded that ride quality for the passive vehicle travelling at 340 km/h would be unacceptable.
On the other hand, the P_{CT} values obtained at 340 km/h for all considered configurations of the actively controlled vehicle are lower than the PCT obtained for the passive vehicle at 300 km/h. At the same time, the rms of lateral acceleration for the active vehicle travelling at 340 km/h is only slightly increased with respect to the value found for the passive vehicle running at 300 km/h and even lower for the PIDSH controller. Therefore, it can be concluded that the introduction of active capabilities allows to raise the speed of the vehicle in the considered curve to 340 km/h without involving significant degradation of ride quality.
The performances in terms of tracking of the references are shown in Figures 10 and 11, considering respectively roll and lateral motion. Both PID and PIDSH controllers show good tracking properties in terms of promptness and maximum errors. The LQ controller, on the contrary, is the slowest to react to a reference variation. This is due to the lack of feed-forward component in the control action, since the integral contribution represents the sub-optimal implementation of the tracking contribution in a LQ controller [35]. In the choice of the final controllers, tracking of the roll reference was prioritised with respect to tracking of the lateral reference because an error on the tilt angle directly affects ride quality, whereas the control of the lateral position of the carbody is intended to avoid bumpstop contact which can be achieved as long as the tracking error is smaller than the bumpstop dead zone, which is assumed to be ±35 mm for the considered vehicle.

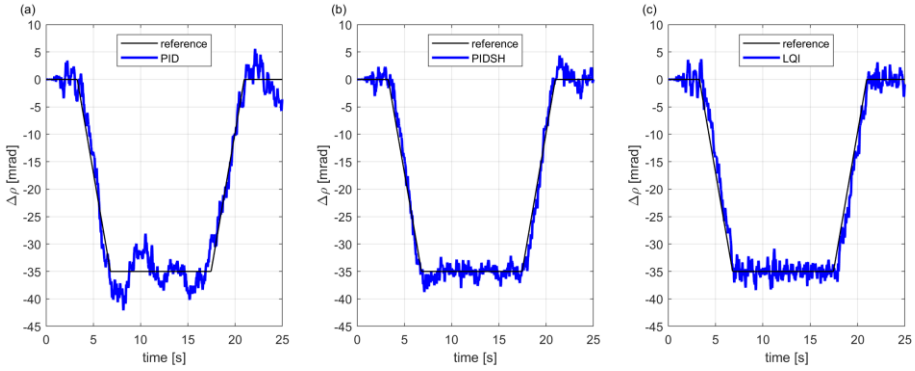

Figure 10. Tilt reference tracking for the optimised active system configurations.

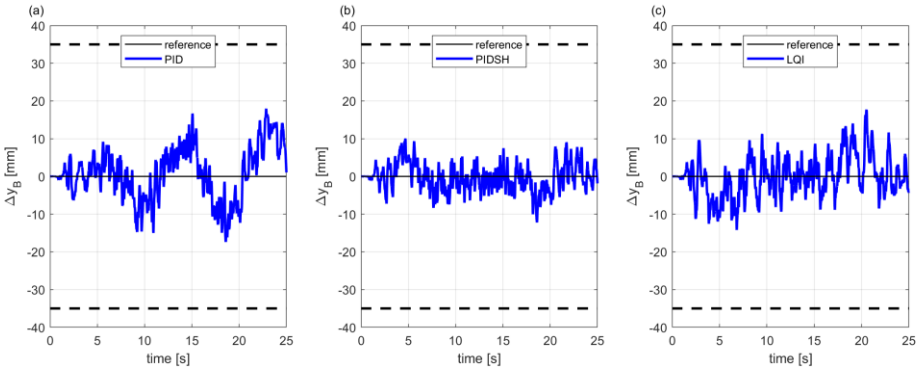

Figure 11. Lateral reference tracking for the optimised active system configurations.

The influence of the active secondary suspension on the vehicle's running safety was investigated as well. In particular, derailment and rollover coefficients were computed in order to assess the safety of the tilting vehicle as prescribed by the standards currently in use [36,37]. The maximum values of the derailment coefficient measured on all the wheels $(Y/Q)_{max}$ together with the maximum value of the rollover coefficient η are reported in Table 5 considering the different controller options and, as reference, the conventional vehicle negotiating the usual curve at two speeds: the traditional 300 km/h and the same (340 km/h) of the vehicle in active configuration.

The increase of speed from 300 to 340 km/h inevitably leads to an increase of the derailment coefficient which is due to the larger non-compensated acceleration, but the influence of active control on this value is basically neutral, as the maximum derailment coefficients obtained for various version of the controller are either slightly lower or only slightly higher than the value obtained for the passive vehicle travelling at 340 km/h. On the contrary active control of the lateral position of the carbody allows to reduce the transfer load to the outer wheels due to the centering effect of the active suspension keeping the same level of the rollover coefficient despite an increase of speed up to 40 km/h.

	$(Y/Q)_{max}$	η
Passive (V=300 km/h)	0.467	0.233
Passive (V=340 km/h)	0.622	0.311
PID (indip.) (V=340 km/h)	0.620	0.372
PID (int.) (V=340 km/h)	0.652	0.384
PIDSH (int.) (V=340 km/h)	0.597	0.315
LQ (int.) (V=340 km/h)	0.554	0.336

Table 5. Safety indexes for the optimised active system configurations.

Another issue worth of notice is the power required by the active suspension to perform the tilting manoeuvre. Denoting by η_P the efficiency of the pump (for which a value of 0.85 is assumed), the total power required by the active tilt unit and by the lateral suspension in the vehicle can be computed summing the contributions on the leading and trailing bogies:

$$W = (Q_L + Q_T)\frac{\Delta P}{\eta_P} \tag{18}$$

where Q_L and Q_T are the oil flow rates required by the active system on the leading and trailing bogie respectively and ΔP is the operating pressure drop equal to 196 bar (see Section 2.1), assuming the hydraulic circuit does not recover energy from the return fluid.
Table 6 reports the rms and maximum values of the power W.

Controller	***rms(W)* [kW]**	***max(W)* [kW]**
PID (indip.)	2.27	5.24
PID (int.)	2.06	4.83
PIDSH (int.)	5.78	15.94
LQ (int.)	4.68	13.01

Table 6. Power consumption of the optimised active system configurations.

It is apparent that the PID controller is the less demanding one. It is worth noticing that the integrated version shows approximately the same power request of the independent one despite achieving better comfort performances. The PIDSH controller requires the largest power on account of the skyhook damping contribution but is able to provide a significant improvement of comfort. Finally, the power demand associated to the LQ controller is comparable to the PIDSH but the performance levels provided by LQ are significantly worse than for PIDSH. This confirms the complexity in the optimisation of the LQ controller.
The generation of references for the tilting system and lateral suspension was initially assumed to be perfectly synchronised with the position of the vehicle along the curve, thanks to the use of train geo-localisation (via GPS) combined with a data-base of track geometry. The effect of an error on the position of the vehicle along the track and, therefore, an error in the generation of the reference signals may degrade the performances of the active system. With this respect the study was completed considering the performances in presence of a positioning error up to 50 m, which is

larger than the horizontal error obtained using GPS [38]. For the sake of brevity, this analysis is only presented for the "PID (indip.)" controller.
Table 7 reports the values of the performance indexes for five cases, i.e. ideal positioning, ±10 m positioning error, compatible with GPS systems maximum error [38] and ±50 m positioning error. This last value corresponds to the limit to fulfil the European Train Control System (ETCS) requirements [39], considering 1 km balise distance. It is observed that the increase of the rms lateral acceleration is limited in all cases, whereas the P_{CT} index is increased significantly for a positioning error of ±50 m, which is due to increased roll rate of the car body in curve transitions caused by the imperfect synchronisation of the tilt command to the curve transitions. The maximum error on roll increases on account of the positioning error. Note that the roll deviation is evaluated with respect to the ideal tilt (i.e. considering ideal positioning) while the controller keeps the ability to correctly follow the reference that is affected by the positioning error. The errors on the lateral carbody-bogie displacement slightly increase since the error on the reference signal is directly affecting the feed-forward contribution.

Reference	P_{CT} **[%]**	$rms(\ddot{y})$ **[m/s²]**	$rms(x_{dR})$ **[%]**	$max(\varepsilon_R)$ **[mrad]**	$rms(x_{dL})$ **[%]**	$max(\varepsilon_L)$ **[mm]**
Ideal	2.220	0.217	5.76	8.9	3.93	21.0
10 m delay	2.499	0.233	5.50	8.9	2.84	23.6
10 m advance	2.334	0.224	5.52	8.8	3.17	26.9
50 m delay	4.035	0.240	5.56	9.7	2.58	20.4
50 m advance	3.532	0.248	5.65	10.5	4.10	34.8

Table 7. Performances of the PID configuration in presence of positioning errors.

6 Conclusions

This paper presented the integration between an active hydraulic tilting system and an active lateral suspension in a high-speed railway vehicle. The objective of the active system is to provide a limited amount of tilt without involving a major re-design of the vehicle. The system has been designed in order to overcome the main drawback of tilting body systems based on active airspring control that is a large consumption of compressed air and hence of energy. The results presented in the paper show that the relatively simple and energy-effective system makes possible raising the running speed from 300 to 340 km/h in high-speed line curves , achieving the same or even slightly improved comfort of passengers. The main cons associated with the system proposed in the paper are the need to incorporate a hydraulic circuit in the vehicle (thus an increased complexity of the system which may lead to a reduction of the reliability) and to update the design of the secondary suspension to make it compliant to the requirements of the tilting system (e.g. in terms of maximum elongation of the airsprings and minimum working height).
It is shown that the integration of the two subsystems leads to significant improvements in the performance of the active suspension due to the coupling between roll and lateral motion of the carbody.

Different control strategies have been implemented with the goal of raising to 340 km/h the vehicle's service speed in typical high-speed curves, maintaining the same level of ride quality of the passive vehicle running at 300 km/h and avoiding motion sickness problems that tipically arise with tilting-body vehicles.
The effectiveness of the proposed solutions has been assessed by means of numerical simulations of the running dynamics of a high-speed train. Numerical simulations were also used in order to fine-tune the gains of the different control strategies by means of a multi-objective optimisation performed using a genetic algorithm. Different conflincting objectives represented by sinthetical indexes were considered related to passenger comfort, tracking performances and control effort.
Three controllers were considered for the active suspension: PID, PIDSH and LQ. The simple PID regulator provides satisfactory results (P_{CT}=2.220 and $rms(\ddot{y})$=0.217 m/s^2, compared to P_{CT}=3.089 and $rms(\ddot{y})$=0.190 m/s^2 for the passive vehicle at 300 km/h) and the addition of the sky-hook damping contribution further improves ride quality ($rms(\ddot{y})$ reduced to 0.183 m/s^2) but requires an increased control effort. On the contrary, the LQ regulator was less performant (P_{CT}=2.926 and $rms(\ddot{y})$=0.252 m/s^2) with respect to PID schemes on account of two main reasons: firstly the lack of a feed-forward action reduces the promptness of the controller and secondly the variables which are optimised are not directly the gains of the controller but the weights in the matrices appearing in the Riccati equation that defines the LQ controller.
The power required to perform the tilting manoeuvre ranges from around 2.06 kW (rms value) for the PID strategy up to 5.78 kW considering the most effective PIDSH version. Even the largest power required for the PIDSH is compatible with a relatively compact design of the actuation system.
All the control strategies rely on a geo-localisation system for the generation of the reference for the controller. It was shown that even considering a positioning error of 50 m the performances of the controllers are not compromised.
Finally, from a safety point of view, it was found that the control strategies are not degrading the running behaviour of the vehicle, so that a sufficient safety margin is kept in regard to running safety even considering the targeted speed increase.

References

[1] Goodall R. Active railway suspensions: Implementation status and technological trends. Veh. Syst. Dyn. 1997;28:87–117.
[2] Bruni S, Goodall R, Mei TX, et al. Control and monitoring for railway vehicle dynamics. Veh. Syst. Dyn. 2007;45:743–779.
[3] Tanifuji K, Koizumi S, Shimamune RH. Mechatronics in Japanese rail vehicles: Active and semi-active suspensions. Control Eng. Pract. 2002;
[4] Fu B, Giossi RL, Persson R, et al. Active suspension in railway vehicles: a literature survey. Railw. Eng. Sci. 2020 281. 2020;28:3–35.
[5] Persson R, Goodall RM, Sasaki K. Carbody tilting - Technologies and benefits. Veh. Syst. Dyn. 2009;
[6] Iwnicki S (Simon), Spiryagin M, Cole C, et al. Handbook of railway vehicle dynamics.
[7] Nakakura Y, Hayakawa K. The body inclining system of the series N700 Shinkansen. Int. Symp. Speed-up, Saf. Serv. Technol. Railw. Maglev Syst. 2009. The Japan Society of Mechanical Engineers; 2009.
[8] Alfi S, Bruni S, Diana G, et al. Active control of airspring secondary suspension

to improve ride quality and safety against crosswinds. Proc. Inst. Mech. Eng. Part F J. Rail Rapid Transit. 2011;
[9] Colombo EF, Di Gialleonardo E, Facchinetti A, et al. Active carbody roll control in railway vehicles using hydraulic actuation. Control Eng. Pract. 2014;31:24–34.
[10] Orvnas A, Stichel S, Persson R. Active lateral secondary suspension with H∞ control to improve ride comfort: Simulations on a full-scale model. Veh. Syst. Dyn. 2011;
[11] Zhou R, Zolotas A, Goodall R. Integrated tilt with active lateral secondary suspension control for high speed railway vehicles. Mechatronics. 2011;21:1108–1122.
[12] Ho WK, Lim KW, Xu W. Optimal Gain and Phase Margin Tuning for PID Controllers. Automatica. 1998;34:1009–1014.
[13] Hägglund T, Panagopoulos H, Åström KJ. Design of PID controllers based on constrained optimisation. IEE Proc. - Control Theory Appl. 2002;149:32–40.
[14] Daniyan IA, Mpofu K, Osadare DF. Design and simulation of a controller for an active suspension system of a rail car. Guo J, editor. Cogent Eng. 2018;5.
[15] Hassan F, Zolotas A. Impact of fractional order methods on optimized tilt control for rail vehicles. Fract. Calc. Appl. Anal. 2017;20.
[16] Di Gialleonardo E, Santelia M, Bruni S, et al. A simple active carbody roll scheme for hydraulically actuated railway vehicles using internal model control. ISA Trans. 2021;
[17] Zhang N, Smith WA, Jeyakumaran J. Hydraulically interconnected vehicle suspension: background and modelling. Veh. Syst. Dyn. 2010;48:17–40.
[18] Merritt HE. Hydraulic control systems. John Wiley and Sons; 1967.
[19] Otegui J, Bahillo A, Lopetegi I, et al. A Survey of Train Positioning Solutions. IEEE Sens. J. 2017;17:6788–6797.
[20] Cangioli, Filippo; Carnevale, Marco; Chatterton, Steven; De Rosa, Anna; Mazzola L. Experimental results on condition monitoring of railwayinfrastructure and rolling stock. Proc. First World Congr. Cond. Monit. (WCCM 2017). London; 2017. p. 1–12.
[21] Wen-Hong Zhu, Lamarche T. Velocity Estimation by Using Position and Acceleration Sensors. IEEE Trans. Ind. Electron. 2007;54:2706–2715.
[22] Bruni S, Collina A, Diana G, et al. Lateral dynamics of a railway vehicle in tangent track and curve: Tests and simulation. 2000;33:464–477.
[23] Braghin F, Bruni S, Diana G. Experimental and numerical investigation on the derailment of a railway wheelset with solid axle. Veh. Syst. Dyn. 2006;44:305–325.
[24] ERRI: B176/3 Benchmark problem — Results and assessment. 1993.
[25] Di Gialleonardo E, Braghin F, Bruni S. The influence of track modelling options on the simulation of rail vehicle dynamics. J. Sound Vib. 2012;331:4246–4258.
[26] Fleming P., Purshouse R. Evolutionary algorithms in control systems engineering: a survey. Control Eng. Pract. 2002;10:1223–1241.
[27] Baumal AE, McPhee JJ, Calamai PH. Application of genetic algorithms to the design optimization of an active vehicle suspension system. Comput. Methods Appl. Mech. Eng. 1998;163:87–94.
[28] He Y, McPhee J. Multidisciplinary design optimization of mechatronic vehicles with active suspensions. J. Sound Vib. 2005;283:217–241.
[29] Tsao YJ, Chen R. The design of an active suspension force controller using genetic algorithms with maximum stroke constraints. Proc. Inst. Mech. Eng. Part

D J. Automob. Eng. 2001;215:317–327.
[30] Zamzuri H, Zolotas AC, Goodall RM. Tilt control design for high-speed trains: a study on multi-objective tuning approaches. Veh. Syst. Dyn. 2008;46:535–547.
[31] Deb K, Agrawal S, Pratap A, et al. A Fast Elitist Non-dominated Sorting Genetic Algorithm for Multi-objective Optimization: NSGA-II. Springer, Berlin, Heidelberg; 2000. p. 849–858.
[32] EN 12299 Railway Applications - Ride comfort for passengers - Measurement and evaluation. 2009. p. 62.
[33] Goldberg DE. Genetic algorithms in search, optimization, and machine learning. Addison-Wesley Longman Publishing Co., Inc.; 1989.
[34] Goldberg DE. The design of innovation : lessons from and for competent genetic algorithms. Kluwer Academic Publishers; 2002.
[35] Lewis FL, Vrabie DL, Syrmos VL. Optimal Control. John Wiley & Sons; 2012.
[36] EN 14067 Railway Applications – Aerodynamics – Part 6: Requirements and Test Procedures for Cross Wind Assessment. 2010.
[37] EN 14363 Railway applications. Testing and Simulation for the acceptance of running characteristics of railway vehicles. Running Behaviour and stationary tests. 2016.
[38] Center WJHT. Global Positioning System (GPS) Standard Positioning Service (SPS) Performance Analysis Report. 2014.
[39] Ansaldo A, Invensys B, Thales S. Performance Requirements for Interoperability Company Technical Approval Management approval.

Appendix 1

With reference to Figure 1, assuming a closed system ($Q_{s1} = Q_{s2} = 0$) and neglecting the leakages ($c_i = c_e = 0$), Equation (1) becomes

$$\begin{cases} \left(\frac{V_0}{\beta} + \frac{A\,x}{\beta}\right)\dot{p}_1 = -A\dot{x} \\ \left(\frac{V_0}{\beta} - \frac{A\,x}{\beta}\right)\dot{p}_2 = +A\dot{x} \end{cases} \tag{A1.1}$$

Neglecting second order terms and and taking the difference of the Equations A1.1

$$\frac{V_0}{\beta}(\dot{p}_1 - \dot{p}_2) = -2A\dot{x} \tag{A1.2}$$

Integrating A1.2

$$(p_1 - p_2) = -2\frac{\beta}{V_0}Ax \tag{A1.3}$$

Considering roll actuators and assuming small perturbations around equilibrium position so to linearise the kinematics

$$x = \frac{b_\rho}{2}\Delta\rho \tag{A1.4}$$

$$V_0 = V_{\rho 0} \tag{A1.5}$$

$$A = A_\rho \tag{A1.6}$$

The force generated by the roll actuators can be obtained:

$$F_\rho = A_\rho(p_{\rho 1} - p_{\rho 2}) = A_\rho\left(-2\frac{\beta}{V_{\rho 0}}A_\rho\frac{b_\rho}{2}\Delta\rho\right) = -\frac{A_\rho^2 b_\rho}{V_{\rho 0}}\beta\Delta\rho \tag{A1.7}$$

Assuming that the two roll actuators generate equal and opposite force (due to the interconnection between the chambers), leading to the expression of k_ρ as reported in Equation 6:

$$M_\rho = F_\rho b_\rho = -\frac{A_\rho^2 b_\rho^2}{V_{\rho 0}}\beta\Delta\rho = -k_\rho\Delta\rho \tag{A1.8}$$

On the other hand, considering lateral actuator and assuming small perturbations around equilibrium position so to linearise the kinematics:

$$x = x_y \tag{A1.9}$$

$$V_0 = V_{y0} \tag{A1.10}$$

$$A = A_y \tag{A1.11}$$

The force generated by the lateral actuator can be obtained, leading to the expression of k_y as reported in Equation 6:

$$F_y = A_y\left(p_{y1} - p_{y2}\right) = A_y\left(-2\frac{\beta}{V_{y0}}A_y x_y\right) = -2\frac{A_y^2}{V_{y0}}\beta x_y = -k_y x_y \qquad \text{(A1.12)}$$

Appendix 2

$$
\begin{cases}
m\ddot{x} = -2c_v\dot{x} - 2k_v x \\
m\ddot{y} = -c_l\dot{y} - c_l h_l\dot{\rho} - k_l y - k_l h_l \rho - A_y\left(p_{y1} - p_{y2}\right) \\
J_\rho\ddot{\rho} = -c_l h_l\dot{y} - (c_l h_l^2 + c_v b_v^2)\dot{\rho} - k_l h_l y - (k_l h_l^2 + k_v b_v^2)\rho - A_y h_y\left(p_{y1} - p_{y2}\right) - A_\rho b_\rho\left(p_{\rho 1} - p_{\rho 2}\right) \\
\frac{2V_{\rho 0}}{\beta}\dot{p}_{\rho 1} = -A_\rho b_\rho\dot{\rho} - \left(c_{i\rho} + c_{e\rho}\right)p_{\rho 1} + c_{i\rho}p_{\rho 2} + K_{q\rho}x_{s\rho} \\
\frac{2V_{\rho 0}}{\beta}\dot{p}_{\rho 2} = +A_\rho b_\rho\dot{\rho} + c_{i\rho}p_{\rho 1} - \left(c_{i\rho} + c_{e\rho}\right)p_{\rho 2} - K_{q\rho}x_{s\rho} \\
\frac{V_{y0}}{\beta}\dot{p}_{y1} = +A_y\dot{y} + A_y h_y\dot{\rho} - \left(c_{iy} + c_{ey}\right)p_{y1} + c_{iy}p_{y2} + K_{qy}x_{sy} \\
\frac{V_{y0}}{\beta}\dot{p}_{y2} = +A_y\dot{y} + A_y h_y\dot{\rho} + c_{iy}p_{y1} - \left(c_{iy} + c_{ey}\right)p_{y2} - K_{qy}x_{sy} \\
\dot{x}_{s\rho} = -\frac{1}{\tau_s}x_{s\rho} + \frac{k_s}{\tau_s}u_{s\rho} \\
\dot{x}_{sy} = -\frac{1}{\tau_s}x_{sy} + \frac{k_s}{\tau_s}u_{sy}
\end{cases}
\tag{A2.1}
$$